Kinetics of the Reactions of the Criegee Intermediate CH_2OO with Water Vapour: Experimental Measurements as a Function of Temperature and Global Atmospheric Modelling

Rachel E. Lade,[a] Mark A. Blitz,[a,b] Matthew Rowlinson,[c] Mathew J. Evans,[c,d] Paul W. Seakins,[a] and Daniel Stone*[a]

[a] School of Chemistry, University of Leeds, Leeds, LS2 9JT, UK

[b] National Centre for Atmospheric Science, University of Leeds, Leeds, LS2 9JT, UK

[c] Wolfson Atmospheric Chemistry Laboratories, Department of Chemistry, University of York, York YO10 5DQ, UK

[d] National Centre for Atmospheric Science, University of York, York YO10 5DQ, UK

* Corresponding author

Email: d.stone@leeds.ac.uk

Supplementary Information

1. Hygrometer Calibration and Measurements of Water Vapour

Water was introduced into the reaction system by passing a flow of N_2 through a bubbler containing deionised water and then combined with the N_2-O_2 in a gas manifold using calibrated mass flow controllers (MFCs). The water vapour concentration was measured using relative humidity (RH) probes (Michell Instruments PCMini 52) that were calibrated against a dew point hygrometer (Buck Research Instruments, CR-4 chilled mirror hygrometer) for RH between 0 and 80 % (Figure S1).

Experiments involving two calibrated RH probes (RH1 and RH2) were carried out to ensure that no water vapour was being lost throughout the experimental apparatus. The first probe (RH1) was placed at the exit of the reaction cell at all times (where RH measurements were made for the experiments), and the second probe (RH2) was initially placed at the end of the gas mixing manifold, and then moved to the entrance of the reaction cell. For each position of RH2, the flow through the water bubbler was increased and decreased, whilst maintaining a total flow of 3.7 standard litres per minute and comparisons between RH1 and RH2 were made. Under all flow conditions, RH readings from RH1 and RH2 were within the reported error value (0.2 % RH) from each other.

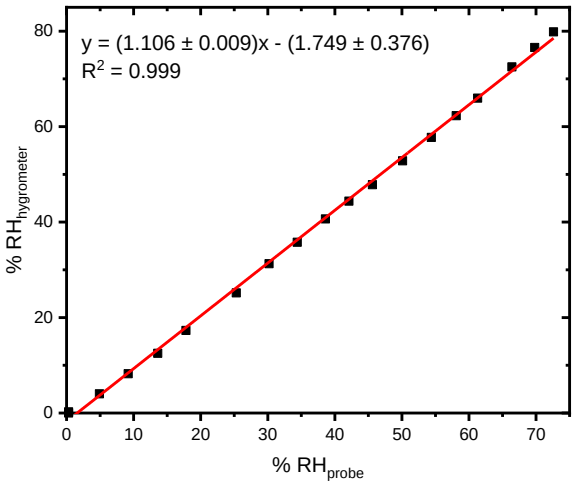

Figure S1. Calibration of the relative humidity (RH) measured with the RH probe used for experiments against the RH measured using a dew point hygrometer. The red line represents a linear fit to the data and gave: gradient = (1.106 ± 0.009), intercept = -(1.749 ± 0.376) and R^2 = 0.999.

2. Instrument Response Function (IRF)

All experiments throughout this work were carried out under pseudo-first-order conditions, where the concentrations of water monomers and dimers were in excess over the concentration of CH_2OO. The change in concentration of CH_2OO can therefore be described by a single exponential decay (ES1).

$$[CH_2OO]_t = [CH_2OO]_0 \times \exp(-k't) \quad \text{(ES1)}$$

where $[CH_2OO]_t$ is the concentration of CH_2OO at time t, $[CH_2OO]_0$ is the concentration of CH_2OO at time zero, and k' is the observed rate coefficient.

For time resolved experiments, the detector was exposed to light for time periods between 10 and 100 μs, and then the photocharge from the ten rows of the illuminated region was binned and summed, and shifted vertically into the adjacent row in the storage region at the same shift rate at which the photocharge was shifted in the illuminated region. As a result of this, the measured temporal profiles of CH_2OO are fit using an equation that describes a convolution of the 'true' kinetic decay of CH_2OO (ES1) with an instrument response function (IRF) described by a Gaussian centred at time t_c with a width w (ES2).[1, 2]

$$[CH_2OO]_t = \frac{[CH_2OO]_0}{2} \exp\left[\frac{(k'w)^2}{2} - k'(t - t_c)\right] \times \left[1 + \text{erf}\left(\frac{t - t_c - k'w^2}{\sqrt{2}w}\right)\right] \quad \text{(ES2)}$$

where erf is the error function acquired through the integration of the normalised Gaussian function.

All data were fit to equations incorporating the instrument response function (ES2).

3. Mixed-Order Analysis

To investigate the suitability of describing the kinetics using a first-order model (as shown in the main text), the data were also analysed using a mixed first- and second-order model (ES3).

$$[CH_2OO]_t = \frac{k'[CH_2OO]_0}{k'\exp^{(k't)} - 2k''[CH_2OO]_0 + 2k''[CH_2OO]_0 exp^{(k't)}} \qquad \text{(ES3)}$$

where $[CH_2OO]_0$ is the CH_2OO concentration at time zero, $[CH_2OO]_t$ is the CH_2OO concentration at time t, k' is the first-order loss component for CH_2OO and k'' is the second-order loss component.

Convolution of the IRF with the mixed first- and second-order kinetic decay (Equation S3), as described above, gives Equation S4:

$$[CH_2OO]_t = \left\{\frac{1}{\left(\frac{1}{[CH_2OO]_0} + \frac{2k''}{k'}\right)}\right\} \exp\left\{\frac{(k'w)^2}{2} - k'(t - t_c) + \frac{2k''}{k'}\right\} \times \frac{\left\{1 + \mathrm{erf}\left(\frac{t - t_c - k'w^2}{\sqrt{2}\,w}\right)\right\}}{2} \qquad \text{(ES4)}$$

Figure S2 compares fitting a typical concentration-time profile for CH_2OO with the first-order model (Equation S2, solid red line) and the mixed first- and second-order model (Equation S4, dashed blue line). Results show less than a 5 % difference between the first-order component obtained from each fit, and we therfore conclude that the data are well-described by pseudo-first-order kinetics.

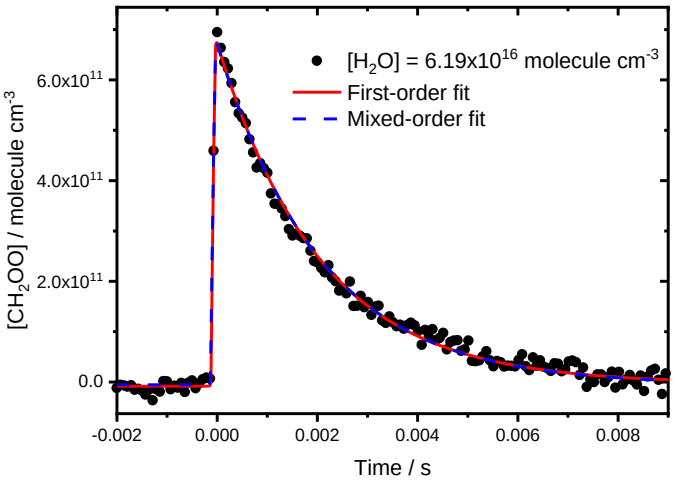

Figure S2. Comparison between a first-order fit (red) and mixed-order fit (blue) for data at 324 K and 760 Torr. The first-order fit gave k' = (728 ± 14) s^{-1} and $[CH_2OO]_0$ = (7.05 ± 0.07) × 10^{11} molecule cm^{-3}. The mixed-order fit gave: k' = (703 ± 10) s^{-1}, k'' = (9.18 ± 0.33) × 10^{-11} cm^3 $molecule^{-1}$ s^{-1}, and $[CH_2OO]_0$ = (7.20 ± 0.22) × 10^{11} molecule cm^{-3}.

4. Concentration–time Profiles for CH_2I_2 and IO

As described in the main text, absorbance spectra obtained in these experiments contain contributions from the precursor, CH_2I_2, and IO formed via secondary chemistry. Figures S3 and S4 show typical concentration-time profiles for both CH_2I_2 and IO obtained in this work. The change in concentration of CH_2I_2, $\Delta[CH_2I_2]$, is negative due to its depletion upon photolysis, and then remains effectively constant on the timescale of the experiment. The concentration-time profile for IO (Figure S4) shows a rapid initial production, followed by a slower production and subsequent decay. The production of IO following the photolysis of CH_2I_2-O_2 has been investigated in a number of previous studies and has been shown to be a result of secondary chemistry involving iodine atoms[3-6] (a more detailed overview can be found in Mir *et al.*[7]).

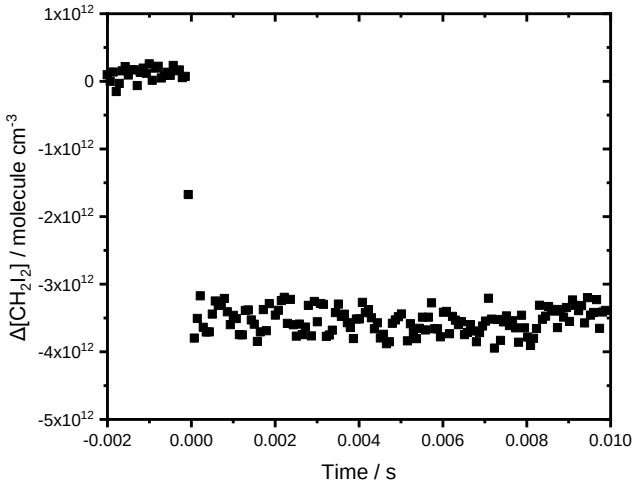

Figure S3. Concentration-time profile for CH_2I_2 for an experiment at 760 Torr and 298 K. For these data, $[H_2O] = 0$, $[CH_2I_2] = 4.1 \times 10^{13}$ molecule cm^{-3}, and $\Delta[CH_2I_2] = 3.5 \times 10^{12}$ molecule cm^{-3}.

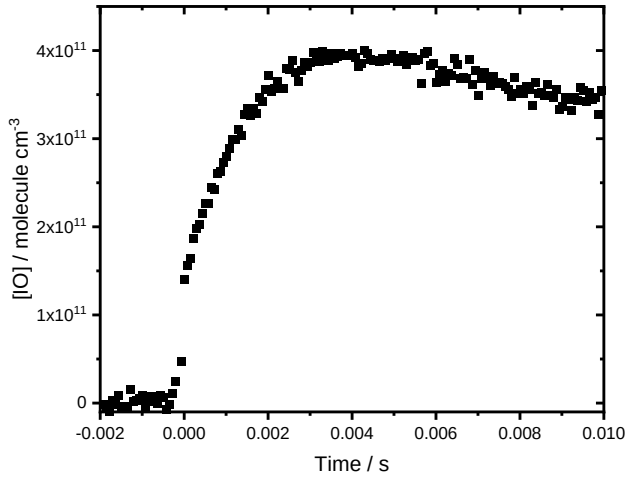

Figure S4. Concentration-time profile for IO for an experiment at 760 Torr and 298 K. For these data, $[H_2O] = 0$ and $[CH_2I_2] = 4.1 \times 10^{13}$ molecule cm^{-3}.

5. Analysis in Terms of $k_{2,eff}$ and Use of Literature Values for K_{eq}^{D}

Describing the reaction using $k_{2,eff}$ ($k_{2,eff} = k_2 K_{eq}^{D}$) is advantageous as it eliminates the potential discrepancy between calculations of the water dimer concentrations resulting from the use of a different value for K_{eq}^{D} to that adopted in this work. When comparing previous experimental investigations of this reaction, it is noted that some studies[8, 9] utilise K_{eq}^{D} values reported by Scribano *et al.*,[10] whereas others,[11-13] including the work presented here, use K_{eq}^{D} values reported by Ruscic *et al.*[14]

Table S1 compares the K_{eq}^{D} values reported by Scribano *et al.* and Ruscic *et al.* for a range of temperatures and demonstrates the differences in calculated water dimer concentrations using the different values for K_{eq}^{D}. The differences in calculated water dimer concentrations impact calculated values for CH_2OO kinetics with water dimers if the kinetics are described in terms of the water dimer concentration directly (i.e. using $rate_{R2} = k_2[CH_2OO][(H_2O)_2]$), leading to errors of up to 25 % if the reference for K_{eq}^{D} is not consistent with that used in this work.

When describing the kinetics of the reaction of CH_2OO with water dimers in terms of water monomer concentrations (i.e. using $rate_{R2} = k_{2,eff}\,[CH_2OO][H_2O]^2$), values for $k_{2,eff}$ reported in this work can be used directly, without need to calculate K_{eq}^{D} separately, thereby reducing the potential for introducing errors in the calculated kinetics.

T / K	[H_2O] / molecule cm^{-3}	K_{eq}^{D} / bar^{-1} (Scribano *et al.* [10])	[$(H_2O)_2$] / molecule cm^{-3}	k' / s^{-1}	K_{eq}^{D} / bar^{-1} (Ruscic *et al.* [14])	[$(H_2O)_2$] / molecule cm^{-3}	k' / s^{-1}	$k'_{Ruscic} / k'_{Scribano}$
262	7.23×10^{16}	0.1471	2.78×10^{13}	803	0.1194	2.25×10^{13}	650	0.81
298	7.63×10^{17}	0.0519	1.24×10^{15}	11767	0.0501	1.20×10^{15}	11388	0.97
353	9.80×10^{18}	0.0150	7.02×10^{16}	188136	0.0187	8.75×10^{16}	234500	1.25

Table S1. A comparison of the Equilibrium constant, K_{eq}^{D}, values reported by Scribano *et al.*[10] and Ruscic *et al.*[14] for water dimer formation at 262, 298 and 353 K, and impacts on calculated water dimer concentrations and pseudo-first-order losses for CH_2OO resulting from reaction with water dimers when described explicitly in terms of water dimer concentrations (i.e. $k' = k_2[(H_2O)_2]$, using values for k_2 determined at each temperature in this work).

6. Investigation of the Potential Reaction between CH_2OO and Three Water Molecules

Kinetics of CH_2OO reactions in the presence of water vapour have been investigated by Wu *et al.*[13] in experiments performed between 290 and 346 K using UV absorption spectroscopy, which demonstrated evidence for a reaction between CH_2OO and three water molecules. Wu *et al.* investigated the behaviour of $(k'-k_0)[H_2O]^{-2}$, where k' and k_0 represent the pseudo-first-order rate coefficients describing the loss of CH_2OO in the presence and absence of water vapour, respectively, and $[H_2O]$ is the water monomer concentration. If the loss of CH_2OO were dominated by reaction with water dimers, $(k'-k_0)[H_2O]^{-2}$ would not be expected to display any dependence on $[H_2O]$, while contributions from monomer reactions would show a negative dependence of $(k'-k_0)[H_2O]^{-2}$ on $[H_2O]$ at low $[H_2O]$, and contributions involving reactions with three water molecules would show a positive dependence of $(k'-k_0)[H_2O]^{-2}$ on $[H_2O]$ at high $[H_2O]$. Results obtained by Wu *et al*. indicated that there is a contribution to the loss of CH_2OO from a reaction involving three water molecules at 298 K which becomes more significant at lower temperatures.

Figure S5 shows the dependence of $(k'-k_0)[H_2O]^{-2}$ on $[H_2O]$ for data obtained at the lowest (262 K) and highest (353 K) temperatures studied in this work and at 298 K, where the dashed blue lines represent the parameterisation reported by Wu *et al*.[13] The data obtained in this work indicate that there is no significant contribution from a reaction involving three water molecules under the conditions employed in this work. To fully investigate the potential role of a reaction involving three water molecules in the atmospheric removal of CH_2OO, further experiments need to be carried out under higher $[H_2O]$, as with the work of Wu *et al.*, where this reaction will be more significant and the relationship between k' and $k_3[H_2O]$ would be more evident on the bimolecular plot.

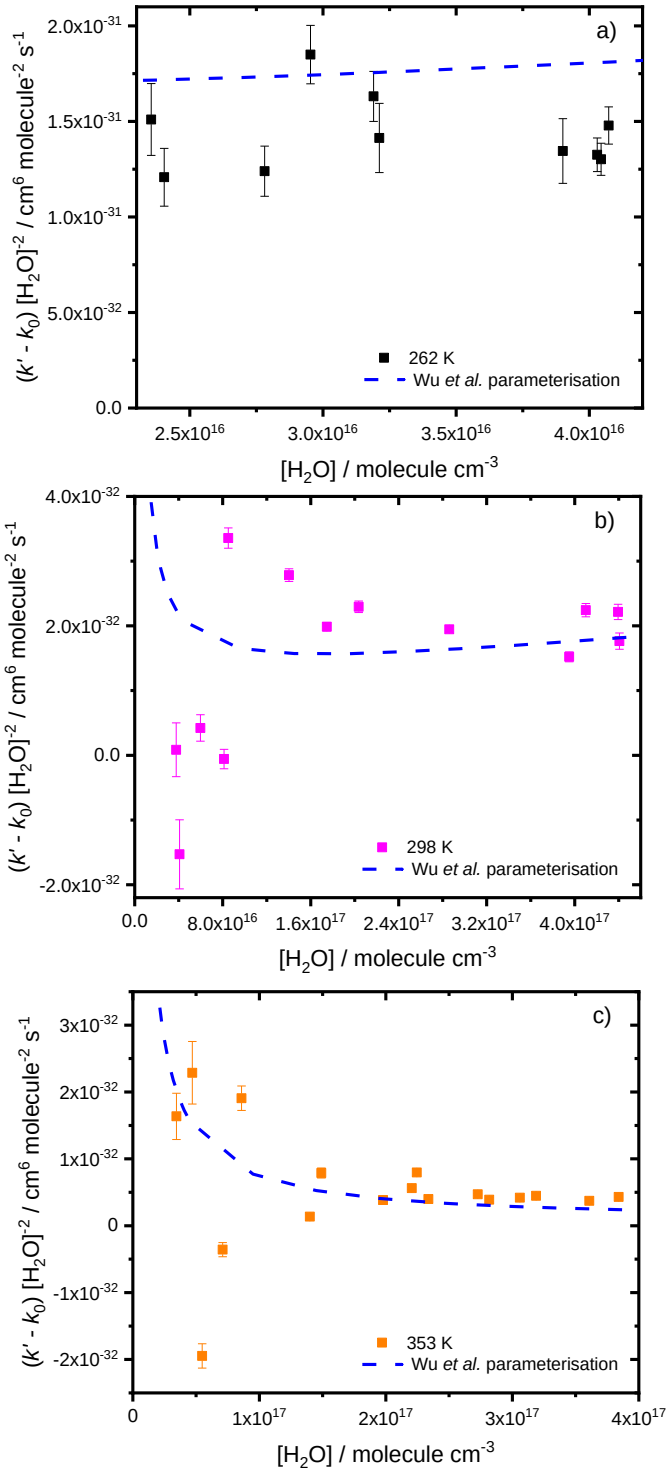

Figure S5. Dependence of $(k'\text{-}k_0)[H_2O]^{-2}$ on $[H_2O]$ for data obtained in this work at a) 262 K, b) 298 K and c) 353 K. The blue dashed line represents the equation $(k' - k_0)[H_2O]^{-2} = k_1[H_2O]^{-1} + k_2 + k_3[H_2O]$, where k_1, k_2 and k_3 were obtained from the work of Wu *et al.*[13]

7. Experimental Uncertainties

The uncertainty in the equilibrium constant, K_{eq}^{D}, taken from Ruscic *et al.*[14] ranges between 2.7 and 3.6 % for the temperature range studied in this work. The RH probe used to determine the water vapour concentration was calibrated using a hygrometer, which gave an uncertainty in the RH readings of 7.9 %. The flow of gases to the reaction cell were controlled using three calibrated MFCs, which gave a combined uncertainty of 5.5 %. On the basis of these uncertainties, we have placed an overall systematic error of 10 % on values of k_1 and $k_{2,eff}$ to account for the uncertainties in the water monomer concentration and a 14 % systematic error on values of k_2 to account for the additional uncertainty of K_{eq}^{D}.

8. Comparison of Global and Local Fit Results for $k_{2,eff}$

Fits described in the main text to find $k_{2,eff}$ were performed globally over all temperatures. Local fits to data at each temperature were unable to retrieve k_1 reliably, but values obtained for $k_{2,eff}$, and Arrhenius parameters for $k_{2,eff}$, from local fits were in good agreement with those obtained in the global fits. Figure S6 shows the comparison between the global fit (which gave $k_{2,eff} = (2.78 \pm 0.28) \times 10^{-38} \exp((4010 \pm 400)/T)$ cm^6 molecule^{-2} s^{-1}) and the local fits (which gave $k_{2,eff} = (2.71 \pm 1.30) \times 10^{-38} \exp((4050 \pm 130)/T)$ cm^6 molecule^{-2} s^{-1}).

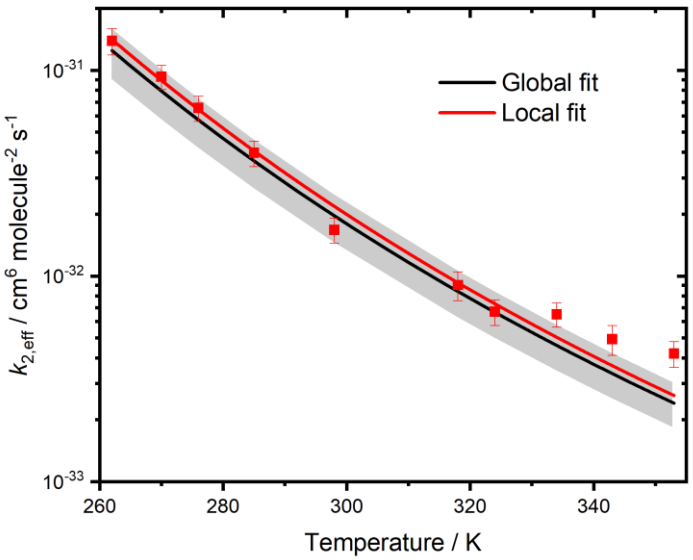

Figure S6. Comparison of the parameterisations for $k_{2,eff}$ using the Arrhenius parameters determined from the global fits (black line, as shown in the main text, with uncertainties shown in the grey shaded region) and the values for $k_{2,eff}$ obtained from local fits to data at each temperature (red points) with the Arrhenius fit (red line). The global fit gave $k_{2,eff} = (2.78 \pm 0.28) \times 10^{-38} \exp((4010 \pm 400)/T)$ cm^6 molecule^{-2} s^{-1} while the local fits gave $k_{2,eff} = (2.71 \pm 1.30) \times 10^{-38} \exp((4050 \pm 130)/T)$ cm^6 molecule^{-2} s^{-1}.

9. Comparison of Observations with Previous Work

Figure S7 compares the total pseudo-first-order losses observed in this work and the work of Wu *et al*. as well as the individual contributions of k_1 and $k_{2,eff}$ from this work and k_1, $k_{2,eff}$ and $k_{3,eff}$ from Wu *et al*. The value for $k_{2,eff}$ reported by Wu *et al.*[13] at 298 K is a factor of ~1.8 lower than that reported here, but there is good agreement in the total pseudo-first-order rate coefficients as a function of water monomer concentration observed in this work and reported by Wu *et al*., and direct comparison of individual terms contributing to the total pseudo-first-order rate coefficients is not entirely appropriate owing to the different numbers of terms included.

Figure S7 (Page S12, below). Pseudo-first-order losses as a function of H_2O concentration for experiments at 262 – 353 K. Black points represent the experimental data, the green and blue solid lines represent losses due to reaction with the water monomer and the water dimer and the solid red line represents the total loss. The results of Wu *et al.*[13] are also included in the plot, where the orange, pink and grey dashed lines represent reactions with the water monomer, dimer and the reaction involving three water molecules, and the purple dashed line represents the total loss. The light blue dotted line on (e) represents $[H_2O] = 4.8 \times 10^{17}$ molecule cm^{-3}, the point at which Wu *et al.* report the reaction with three water molecules becomes significant at 298 K.

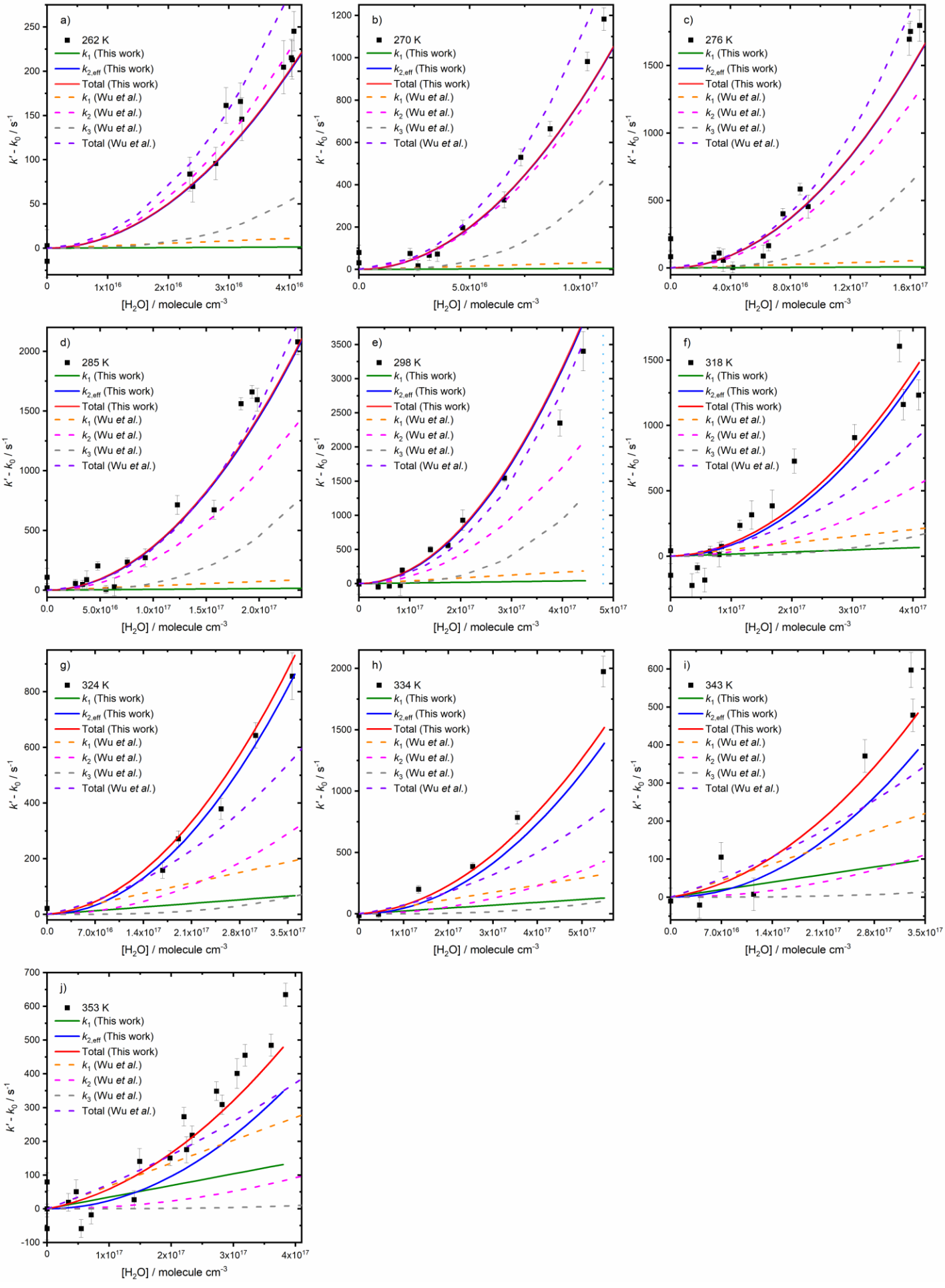
a)
262 K
b)
270 K
c)
276 K
d)
285 K
e)
298 K
f)
318 K
g)
324 K
h)
334 K
i)
343 K
j)
353 K
k_1 (This work)
$k_{2,eff}$ (This work)
Total (This work)
k_1 (Wu et al.)
k_2 (Wu et al.)
k_3 (Wu et al.)
Total (Wu et al.)
$k' - k_0$ / s^{-1}
[H_2O] / molecule cm^{-3}

10. Values for k_1 and $k_{2,eff}$ used in GEOS-Chem Simulations

Figure S8 compares the rate coefficients for the reactions of CH_2OO with H_2O and $(H_2O)_2$ at temperatures between 200 and 400 K used in the three GEOS-Chem model simulations (outlined in Table 4 in the main text).

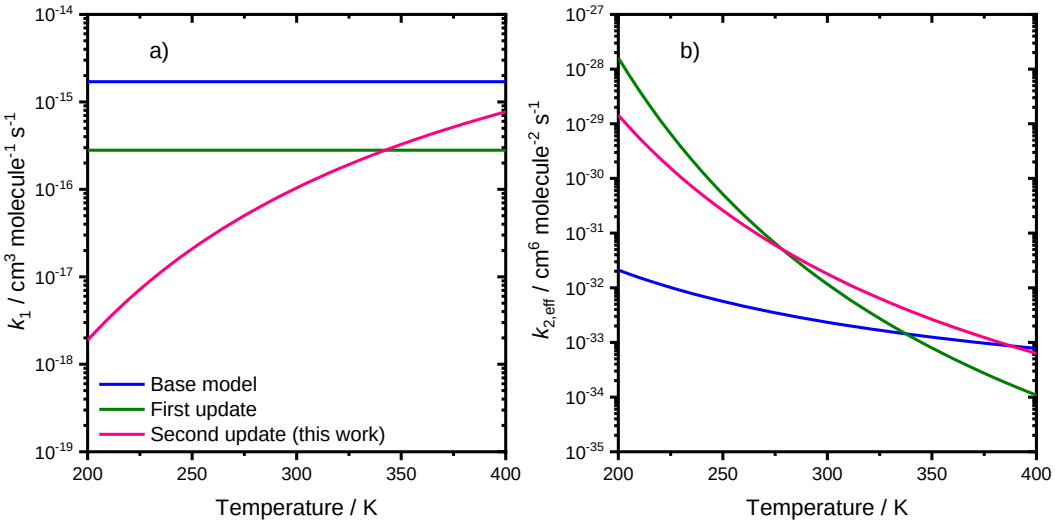

Figure S8. Comparison of rate coefficients used in GEOS-Chem for reactions of CH_2OO with (a) the water monomer and (b) the water dimer at temperatures between 200 and 400 K. Parameterisations are given in the main text.

11. Experimental Data

T / K	$[CH_2I_2]_0$ / 10^{13} molecule cm^{-3}	$[H_2O]$ / 10^{16} molecule cm^{-3}	$[(H_2O)_2]$ / 10^{13} molecule cm^{-3}	k' / s^{-1}	$k' - k_0$ / s^{-1}
262	5.8	0	0	483 ± 10	3 ± 18
		2.40	0.25	550 ± 9	70 ± 17
		2.78	0.34	576 ± 10	96 ± 18
		2.95	0.38	641 ± 13	161 ± 20
		3.21	0.45	626 ± 19	146 ± 24
		3.90	0.66	685 ± 26	205 ± 30
		4.07	0.72	725 ± 16	245 ± 22
262	5.7	0	0	573 ± 7	-15 ± 18
		2.35	0.24	672 ± 10	84 ± 19
		3.19	0.44	754 ± 13	166 ± 21
		4.03	0.70	803 ± 14	215 ± 21
		4.04	0.71	801 ± 14	213 ± 21
270	5.8	0	0	470 ± 6	80 ± 34
		3.54	0.45	463 ± 10	73 ± 35
		4.69	0.79	588 ± 10	198 ± 35
		6.56	1.55	718 ± 17	328 ± 38
		7.31	1.93	920 ± 23	530 ± 40
		10.3	3.84	1372 ± 28	982 ± 44
		11.1	4.42	1573 ± 42	1183 ± 54
270	5.8	0	0	342 ± 11	32 ± 24
		2.31	0.19	386 ± 11	76 ± 24
		2.67	0.26	328 ± 12	18 ± 24
		3.17	0.32	378 ± 14	68 ± 25
		8.64	2.69	975 ± 27	665 ± 34
276	5.9	0	0	620 ± 7	217 ± 83
		3.51	0.39	461 ± 8	58 ± 83
		6.19	1.21	492 ± 10	89 ± 84
		9.18	2.67	858 ± 25	455 ± 87
		15.9	8.02	2098 ± 82	1695 ± 117
		16.6	8.74	2200 ± 83	1797 ± 118
276	6.1	0	0	316 ± 10	84 ± 39
		2.89	0.26	312 ± 9	80 ± 39
		3.24	0.33	343 ± 11	111 ± 39
		4.15	0.54	236 ± 13	4 ± 40
		6.54	1.35	398 ± 15	166 ± 40
		7.51	1.78	635 ± 14	403 ± 40
		8.64	2.36	818 ± 21	586 ± 43
		16.0	8.12	1986 ± 65	1754 ± 75
285	6.2	0	0	572 ± 6	109 ± 74
		3.73	0.37	551 ± 8	88 ± 75
		6.33	1.06	492 ± 9	29 ± 75
		9.26	2.26	736 ± 15	273 ± 76
		12.3	3.97	1177 ± 27	714 ± 79
		15.7	6.53	1137 ± 27	674 ± 79
		19.8	10.3	2058 ± 60	1595 ± 95
		23.6	14.7	2543 ± 79	2080 ± 109
285	6.3	0	0	225 ± 9	20 ± 33
		2.67	0.18	262 ± 9	57 ± 33
		3.34	0.29	253 ± 11	48 ± 34
		4.78	0.60	408 ± 11	203 ± 34
		5.54	0.81	212 ± 9	7 ± 33
		7.57	1.51	441 ± 13	236 ± 34

		18.3	8.80	1766 ± 39	1561 ± 50
		19.3	9.82	1866 ± 43	1661 ± 54
298	4.1	0	0	522 ± 5	32 ± 41
		3.77	0.29	445 ± 6	-45 ± 41
		5.97	0.74	459 ± 7	-31 ± 41
		8.51	1.49	687 ± 11	197 ± 42
		14.0	4.06	991 ± 19	501 ± 45
		17.5	6.30	1051 ± 20	561 ± 45
		28.6	16.9	2035 ± 34	1545 ± 53
298	6.4	0	0	313 ± 7	-5 ± 148
		8.12	0.14	292 ± 10	-26 ± 148
		20.4	0.86	1247 ± 37	929 ± 152
		39.5	0.32	2669 ± 120	2351 ± 190
		44.1	0.40	3722 ± 245	3404 ± 286
318	4.2	0	0	496 ± 18	-146 ± 91
		3.52	0.18	418 ± 19	-224 ± 91
		5.63	0.47	460 ± 24	-182 ± 92
		7.99	0.95	654 ± 29	-13 ± 93
		13.4	2.64	958 ± 63	316 ± 109
		16.8	4.16	1028 ± 81	386 ± 120
		20.4	6.17	1370 ± 25	728 ± 92
		30.3	13.6	1549 ± 48	907 ± 101
		38.4	21.8	1803 ± 77	1161 ± 117
		40.9	24.7	1875 ± 74	1233 ± 116
318	3.8	0	0	585 ± 9	43 ± 36
		4.42	0.29	455 ± 13	-87 ± 37
		6.56	0.64	581 ± 16	39 ± 38
		8.40	1.04	616 ± 18	74 ± 39
		11.4	1.93	779 ± 22	237 ± 41
		37.8	21.1	2148 ± 114	1606 ± 119
324	4.1	0	0	590 ± 11	21 ± 28
		16.8	3.8	728 ± 14	159 ± 29
		19.1	4.92	841 ± 13	272 ± 29
		25.3	8.65	949 ± 27	380 ± 37
		30.3	12.4	1212 ± 38	643 ± 46
		35.6	17.2	1425 ± 80	856 ± 84
334	4.2	0	0	465 ± 8	-13 ± 28
		4.37	0.22	475 ± 7	-3 ± 28
		13.3	2.08	678 ± 14	200 ± 30
		25.5	7.59	864 ± 16	386 ± 31
		35.5	14.7	1263 ± 46	785 ± 53
		54.8	35.1	2453 ± 122	1975 ± 125
343	4.8	0	0	385 ± 12	-10 ± 34
		3.98	0.17	375 ± 14	-20 ± 35
		6.93	0.50	500 ± 21	105 ± 39
		11.4	1.35	402 ± 28	8 ± 43
		26.7	7.40	766 ± 28	371 ± 43
		33.0	11.3	992 ± 33	597 ± 46
		33.3	11.5	874 ± 28	479 ± 43
353	4.8	0	0	532 ± 4	80 ± 26
		3.44	0.11	471 ± 4	19 ± 26
		5.48	0.27	394 ± 5	-58 ± 26
		7.11	0.46	434 ± 5	-18 ± 26
		14.0	1.79	479 ± 7	27 ± 27
		22.1	4.44	725 ± 9	273 ± 27
		27.3	6.79	801 ± 10	349 ± 28

		31.9	9.28	907 ± 19	455 ± 32
		36.1	11.9	937 ± 20	485 ± 33
		38.4	13.5	1087 ± 22	635 ± 34
353	5.1	0	0	468 ± 13	0 ± 14
		19.8	3.57	618 ± 22	150 ± 22
		23.4	4.98	686 ± 28	218 ± 28
		28.2	7.25	777 ± 28	309 ± 29
353	5.5	0	0	502 ± 8	-58 ± 35
		4.70	0.20	611 ± 10	51 ± 35
		14.9	2.03	701 ± 17	141 ± 38
		22.5	4.60	735 ± 20	175 ± 39
		30.6	8.55	961 ± 29	401 ± 44

Table S2. Experimental data obtained in this work. All experiments were carried out at a total pressure of 760 Torr. Values for k_0 for each dataset at constant T and CH_2I_2 concentration were determined from the fits to k' as a function of water monomer concentration.

11. References

1. C. Robinson, L. Onel, J. Newman, R. Lade, K. Au, L. Sheps, D. E. Heard, P. W. Seakins, M. A. Blitz and D. Stone, *The Journal of Physical Chemistry A*, 2022, **126**, 6984-6994.
2. L. Onel, R. Lade, J. Mortiboy, M. A. Blitz, P. W. Seakins, D. E. Heard and D. Stone, *Physical Chemistry Chemical Physics*, 2021, **23**, 19415-19423.
3. W.-L. Ting, C.-H. Chang, Y.-F. Lee, H. Matsui, Y.-P. Lee and J. J.-M. Lin, *The Journal of Chemical Physics*, 2014, **141**, 104308.
4. T. J. Gravestock, M. A. Blitz, W. J. Bloss and D. E. Heard, *Chemical Physics and Physical Chemistry*, 2010, **11**, 3928-3941.
5. T. J. Dillon, M. E. Tucceri, R. Sander and J. N. Crowley, *Physical Chemistry Chemical Physics*, 2008, **10**, 1540-1554.
6. E. S. Foreman and C. Murray, *The Journal of Physical Chemistry A*, 2015, **119**, 8981-8990.
7. Z. S. Mir, T. R. Lewis, L. Onel, M. A. Blitz, P. W. Seakins and D. Stone, *Physical Chemistry Chemical Physics*, 2020, **22**, 9448-9459.
8. T. R. Lewis, M. A. Blitz, D. E. Heard and P. W. Seakins, *Physical Chemistry Chemical Physics*, 2015, **17**, 4859-4863.
9. T. Berndt, J. Voigtländer, F. Stratmann, H. Junninen, R. L. Mauldin III, M. Sipilä, M. Kulmala and H. Herrmann, *Physical Chemistry Chemical Physics*, 2014, **16**, 19130-19136.
10. Y. Scribano, N. Goldman, R. J. Saykally and C. Leforestier, *The Journal of Physical Chemistry A*, 2006, **110**, 5411-5419.
11. M. C. Smith, C.-H. Chang, W. Chao, L.-C. Lin, K. Takahashi, K. A. Boering and J. J.-M. Lin, *The Journal of Physical Chemistry Letters*, 2015, **6**, 2708-2713.
12. W. Chao, J.-T. Hsieh, C.-H. Chang and J. J.-M. Lin, *Science*, 2015, **347**, 751.
13. Y.-J. Wu, K. Takahashi and J. J.-M. Lin, *The Journal of Physical Chemistry A*, 2023, **127**, 9059-8072.
14. B. Ruscic, *The Journal of Physical Chemistry A*, 2013, **117**, 11940-11953.